Efficient Identification of Objects Carrying Elements of High-Order Symmetry By Using Correlated Orbital Angular Momentum (OAM) States

Alexander V. Sergienko[1,4], Néstor Uribe-Patarroyo[1], Andrew Fraine[1], David S. Simon[1,2], and Olga Minaeva[3]

[1]*Dept. of Electrical & Computer Engineering, Boston University, 8 Saint Mary's St., Boston, MA 02215, USA*
[2]*Dept. of Physics and Astronomy, Stonehill College, 320 Washington St., Easton, MA 02357, USA*
[3]*Dept. of Biomedical Engineering, Boston University, 44 Cummington St., Boston, MA 02215, USA*
[4]*Dept. of Physics, Boston University, 590 Commonwealth Avenue, Boston, MA 02215, USA*

Abstract. A major contributions of Wigner's work was the introduction of group theory to study both the dynamics and the classification of states in quantum mechanics. The use of rotational symmetry to study the properties of angular momentum eigenstates is particularly associated with him. Following along a similar path, it is shown here that advances in the study of entangled and correlated two-photon states allow the rapid detection of rotational symmetries in complex macroscopic objects, and that knowledge of this symmetry structure can allow identification, and in some circumstances reconstruction, of the object.

The potential for efficient identification of objects carrying elements of high-order symmetry using correlated orbital angular momentum (OAM) states is demonstrated. The enhanced information capacity of this approach allows the recognition of specific spatial symmetry signatures present in objects with the use of fewer resources than in a conventional pixel-by-pixel imaging, representing the first demonstration of compressive sensing using OAM states. This approach demonstrates the capability to quickly evaluate multiple Fourier coefficients directly linked with the symmetry features of the object. The results suggest further application in small-scale biological contexts where symmetry and small numbers of noninvasive measurements are important.

1 Introduction

The field of correlated sensing, in which the correlation between photons or light beams is used to image an object or to detect its features includes techniques such as ghost imaging [1–4], compressive sensing [5] and compressive ghost imaging [6, 7]. In ghost imaging, correlated light is sent through two different paths, one of which contains the target object and a bucket detector, and the other has a spatially-resolving detector. Correlation between the outputs of each detector allows for the reconstruction of an image or the sensing of particular features of the object [8]. In compressive sensing, the image of the target object is modulated by a number of known (usually random) spatially-varying transmission masks and the output is collected by a bucket detector. An estimation of the object or its

features can be found by correlating the intensity of the detected light with the mask profile. Compressive ghost imaging uses the techniques of compressive sensing in a ghost imaging setup to attain more efficient imaging, such as the recently proposed multiple-input ghost imaging [9], in which the bucket detector is replaced by a sparse-pixelated detector. The importance of compressive sensing stems from the fact that successful sensing of the object requires a number of measurements much smaller than the image size, which has important implications for more efficient remote-sensing techniques.

The use of orbital angular momentum (OAM) states in classical and quantum imaging techniques has been shown to provide additional effects that enhance the sensitivity to particular features of an object. For example, it has been shown that the use of OAM modes in phase imaging configurations increases edge contrast by using a spiral phase distribution as a filter [padgett ghost, spiral phase microscopy] [8]. In addition, digital spiral imaging [10, 11] has been proposed as a technique in which the OAM basis is used to illuminate the object and analyze the transmitted or reflected light. The two-dimensional spatial extent along with the high dimension of the OAM basis set leads to the probing of two-dimensional objects without obtaining a pixel by pixel reconstruction which is analogous to the approach of compressive sensing.

The high dimensionality of the OAM basis combined with the use of correlated two-photon states gives rise to an improved version of digital spiral imaging which exploits the full two-dimensional OAM joint spectrum. This new version is termed correlated spiral imaging (CSI) [12], and is a technique suitable for remote sensing that gathers information from an object by measuring correlated OAM values. The two-photon joint OAM spectrum provides object information in the form of spatial symmetries that yield more efficient object recognition than conventional imaging and sensing techniques. CSI can be viewed as an active version of compressive sensing in which the sampling is performed in the high-dimensional OAM basis. If the object has a compact representation in this basis, a small number of measurements will suffice to identify it.

This paper presents the experimental demonstration of a compressed sensing technique based on OAM states. The present CSI implementation makes use of the expansion in the OAM basis of the states generated by spontaneous parametric down conversion (SPDC) [13–15]. Significant information from the object is available by measuring the *joint* OAM spectrum of two-photon states that gives rise to novel features outside the main diagonal of OAM conservation [16] due to the interaction with the object. In order to use this information for object identification, the direct relationship between the joint spectrum with the Fourier coefficients of the azimuthal and radial characteristics of the object is derived. In the field of remote sensing this capability enables efficient object identification without the requirement of a full two-dimensional image. The present demonstration also represents the first correlated OAM-based sensing experiment representative of a practical remote-sensing setup, in which physical objects completely detached from any optical component are used as test targets for identification. All previous experiments on correlated imaging using OAM states ([8] for example) have used simulated objects drawn on a spatial light modulator (SLM). Clear information and high sensitivity to the spatial properties of the targets are obtained, which demonstrates the high amount of information per photon attainable by the use of CSI.

2 Theoretical basis

Correlated OAM states for the implementation of CSI are created through the process of spontaneous parametric down conversion (SPDC). The two-photon state produced by SPDC can be expressed as an expansion in Laguerre-Gauss (LG) modes $|l, p\rangle$ [14] defined as

$$\langle r, \phi | l, p \rangle = k_p^{|l|} r^{|l|} e^{-r^2/w_0^2} \mathrm{L}_p^{|l|}\left(2r^2/w_0^2\right) e^{i\phi l}, \tag{1}$$
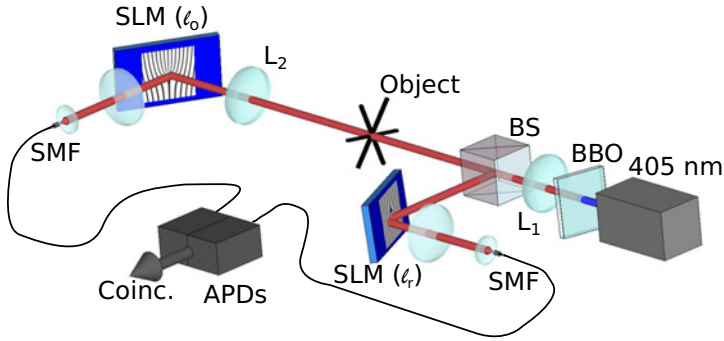
Figure 1. Setup for the sensing of the object via orbital angular momentum of correlated photons.

where $k_p^{|l|}$ is a normalization constant, $L_n^\alpha(x)$ is the generalized Laguerre polymonial of order n and w_0 is the beam waist as defined in this plane. The azimuthal phase term in the LG expression gives rise to modes with quantized OAM of order l. Discrimination between individual radial modes $p \neq 0$ is not attainable by current experimental techniques [17], therefore only the case $p = 0$ will be considered for simplicity and the p index will be dropped hereinafter. This does not affect the generality of the following derivation. In the case of detecting LG modes by the use of holograms and mono-mode fibers [16], the cross-talk given by modes with $p \neq 0$ should be taken into account [14]. In the case of a detection scheme with sensitivity to all p modes [17], projections should consider both the l and p indices.

The total OAM content is known to be conserved in a collinear SPDC process [16], and in the case of a gaussian pump (OAM content $l_p = 0$) the two-photon state can be written as

$$|\Psi\rangle = \sum_{l=-\infty}^{\infty} C_l |-l\rangle |l\rangle, \tag{2}$$

with C_l given by the phase-matching condition and the relation between the pump, signal and idler beam waists [12, 14]. C_l can be viewed as the *natural* OAM spectrum coefficients from SPDC.

Consider the SPDC setup of Fig. 1, where a correlated OAM state is generated after the collinear down-converted beam enters a non-polarizing beam splitter (BS). After splitting, one branch corresponds to the reference arm and the other branch has the object in its path. The stand-alone object is detached from any optical component. The correlated state analyzer is composed of two identical detection systems used to make the *joint* projection on the LG basis. The detectors are connected to a coincidence circuit that analyzes light with OAM number l_r in the reference arm and l_o in the object arm. The coincidence rate is proportional to the *joint spectrum* $P(l_r, l_o)$ of the down-converted beam after interaction with the object. This setup considers the object as a transmissive target, and it is sufficient to reposition the detection unit containing L2 to collect light in reflective mode from the target.

The object is described by a spatially varying transmission and/or phase function $A(r, \phi)$. Interaction of an LG state with the object can be expressed as an operator in the LG basis by the matrix elements of the operator A

$$\langle k|A|l\rangle = A_{kl}. \tag{3}$$

One can calculate $\langle k|A|l\rangle$ (with $\rho = \sqrt{2}r/w_0$) using

$$\langle k|A|l\rangle \qquad = \qquad \sqrt{\frac{2}{\pi|k|!}}\sqrt{\frac{2}{\pi|l|!}} \quad \times \quad \frac{1}{2}\int_0^\infty d\rho \int_0^{2\pi} d\phi \rho^{|k|+|l|+1} e^{-\rho^2} e^{-i\phi(k-l)} A(\rho,\phi). \quad (4)$$

By performing the integration in the radial direction the function $R_{kl}(\phi)$ is obtained, which depends only on the azimuthal variable

$$R_{kl}(\phi) = \frac{2}{\sqrt{|k|!|l|!}} \int_0^\infty d\rho \rho^{|k|+|l|+1} e^{-\rho^2} A(\rho,\phi). \qquad (5)$$

This integration reveals that $R_{kl}(\phi)$ corresponds to the azimuthal features of $A(\rho,\phi)$ weighed at a certain radius of the object. The weight function is the squared absolute value of an LG mode $|l| + |k|$, which is an annular function with its maximum at a radius $w_0\sqrt{(|l| + |k|)/2}$ [18].

The second integration has the form (with $m = k - l$)

$$\langle k|A|l\rangle = \frac{1}{2\pi}\int_0^{2\pi} d\phi e^{-im\phi} R_{kl}(\phi). \qquad (6)$$

Therefore, A_{kl} is the m-th coefficient of the Fourier series of $R_{kl}(\phi)$, the region selected by the "ring" in the first integral. In the setup of Fig. 1, after interaction with the object the two-photon state transforms into (dropping the limits of the summations)

$$|\Psi'\rangle = \sum_l C_l|-l\rangle\left[A|l\rangle\right] = \sum_l C_l|-l\rangle\left[\sum_{k'} A_{k'l}|k'\rangle\right]. \qquad (7)$$

It follows that the joint spectrum is given by

$$P(l_r, l_o) = \langle l_r|\langle l_o||\Psi'\rangle = C_{lr}A_{lr,lo}, \qquad (8)$$

which contains information about the natural SPDC OAM spectrum coefficients C_l as well as information about the object A_{kl}. The OAM spectral signature of the object can be isolated by performing $A_{kl} = P(l,k)/C_l$ for $C_l \neq 0$.

It is important to note that this joint spectrum will have non-zero probability for elements that were previously forbidden by OAM conservation.

Due to the presence of $A_{lr,lo}$, states with $l_r + l_o \neq l_p$ can have non-zero probability. These states were previously forbidden by OAM conservation [13–17] and represents the interaction of the correlated OAM state from SPDC with the object. These new non-conservation elements have a contribution to its total OAM content from the object $m = l_o + l_r - l_p$, and carry direct information of the m-fold rotational symmetries of the object at a $|l_r| + |l_o|$ radius. For instance, considering a gaussian pump ($l_p = 0$), the measured joint spectrum with a m-fold rotationally symmetric target with will show strong components with total OAM content $\pm m$, and higher harmonics with lower amplitudes at nm, $|n| > 1$ being n an integer.

3 Experiment

The experimental setup schematic is shown in Fig. 1. A 1.5 mm-thick BBO crystal is pumped with a 30 mW diode laser at 405 nm. To measure the OAM spectrum, an SLM is used to display computer generated holograms. The holograms change the winding number l of LG light, while two lenses
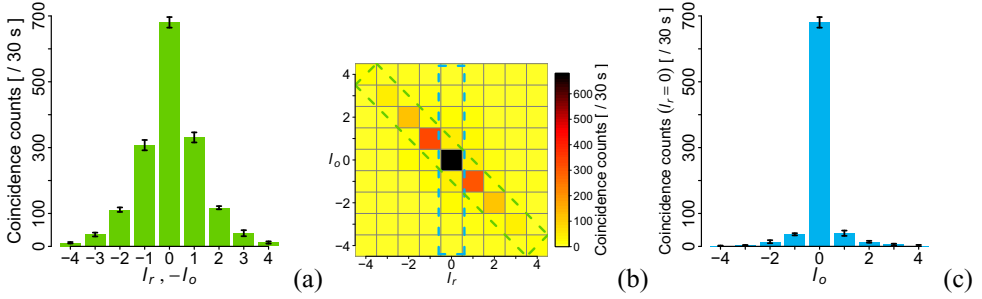
Figure 2. (a) Histogram of the main diagonal and (b) complete two-dimensional OAM joint spectrum for our configuration with no object. (c) Corresponding $P(l_o|l_r = 0)$ cross section. The blue (vertical) box in the joint spectrum denotes the section in (a) and the green (diagonal) box denotes the section in (c).

and a mono-mode fiber selectively couple modes with $l = 0$ [14]. One condition for obtaining A_{kl} without any post-processing is that the projection of Eqs.(4) and (8) are made in equivalent planes. In the current setup, which is a representative demonstration of remote sensing, lens L2 images an object at a fixed distance onto the plane of the SLM. In a general remote sensing application, L2 will be place appropriately so that all targets will be at distances greater than the hyperfocal length of L2. Therefore, all objects will be imaged in focus onto the SLM plane.

Fig. 2 (a–b) illustrates the measurement of the natural SPDC OAM joint spectrum C_l. The sign of l_r is flipped to compensate for the odd number of mirrors in order to reflect the OAM conservation in SPDC. In the absence of an object, the main diagonal terms match the total OAM content of the pump without any non-diagonal terms [15]. Experimental results represent the mean of four measurements, from which the standard deviation is calculated and displayed as error bars. Fig. 2 (c) shows the histogram of the diagonal and the cross section for $P(l_o|l_r = 0)$.

To demonstrate the capability and high sensitivity of this new technique for object recognition, the joint spectra using targets with different rotational symmetries are analyzed. As seen in (8), an object can impart extra features in the joint spectrum according to its azimuthal Fourier series at different radii. In particular, an object with four-fold rotational symmetry will have strong signatures corresponding to a total OAM content of ±4. To fit the scale of our setup, opaque strips 175 μm $(0.83w_0)$ thick, are placed in the object arm arranged with specific rotational symmetries. These targets behave as transmission masks that block light, and the integration time is adjusted in order to have a similar amount of counts with respect to the case of no object. Test objects with well-defined dominant four- and six-fold symmetries shown in Figs. 3 (a) and 4 (a) considerably modify the joint spectra [Figs. 3 (b) and 4 (b)] by adding extra diagonals with total OAM content of $l = ±4$ and $l = ±6$, respectively. The two objects are clearly distinguished by the unique features of their respective joint spectrum.

4 Discussion

All techniques discussed involve *no measurements in position space*. More insight about the structure of each object is acquired by analyzing specific non-diagonal cross sections such as the two in Figs. 3 (d) and 3 (d). Previous work regarding the OAM joint spectrum of SPDC [12–15, 17] have strictly considered the main diagonal elements corresponding to the conservation of OAM with respect to the pump [Figs. 3 (c) and 4 (c)]. In the current case, there is an interaction between the OAM
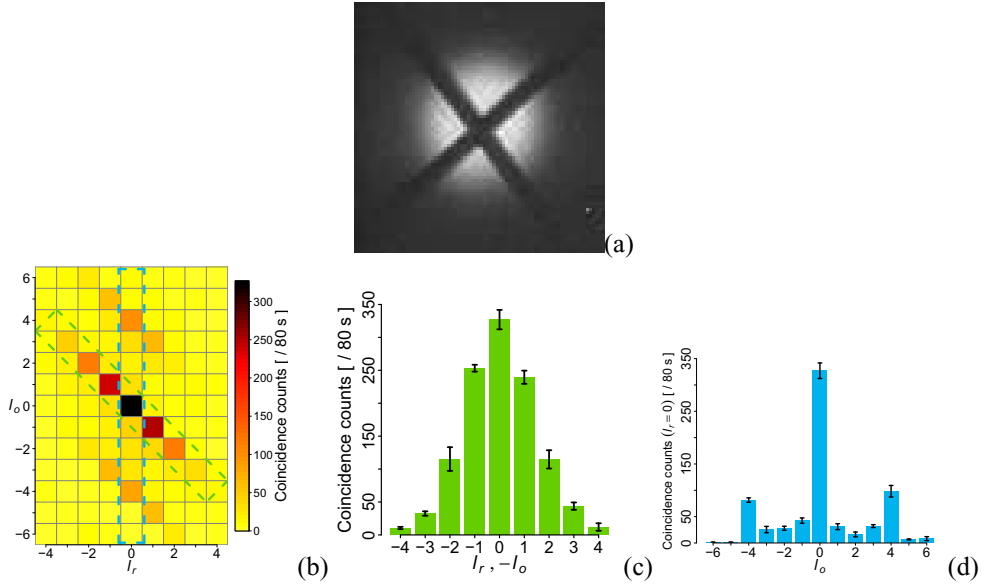
Figure 3. (a) Image of the cross used as target, (b) the experimental joint spectrum, (c) a histogram of the joint spectrum main diagonal and (d) $P(l_o|l_r = 0)$ cross section of the joint spectrum.

from SPDC and the spatial features of the object resulting in contributions which require analysis of the complete two-dimensional joint spectrum.

The non-diagonal cross section $P(l_o|l_r = 0)$ shown in Fig. 3 (d) indicates significant four-fold symmetry as the dominant feature of the object. This feature can be uniquely attributed to the object because it is outside the diagonal that corresponds to the conservation of OAM in SPDC. Fig. 4 (d), showing the same non-diagonal cross section for the six-fold symmetric object, exhibits richer features associated with the higher complexity of the object. Specifically, apart from the dominant six-fold symmetric contribution, a three-fold contribution is observed. At the center of the object [Fig. 4 (a)], the three stripes are displaced with respect to the center. This forms a triangular shape in a small region with three-fold rotational symmetry. This small deviation from a strict six-fold symmetry is readily observed in the non-diagonal cross section by the appearance of significant contributions at $l_o = \pm 3$.

Although the cross section $P(l_o|l_r = 0)$ is a good indicator of the presence of different symmetries, *it is necessary to analyze the full two-dimensional OAM joint spectrum to extract the exact contribution of each symmetry component*. For example, Fig. 4 (d) indicates a relative contribution of six- and three-fold symmetries at a ratio of approximately 2:1. However, to judge the relative size of the areas within the object that exhibit each symmetry, the total contribution of the entire diagonals should be considered. In this case, the joint spectrum in Fig. 4 (b) clearly shows that the region with three-fold symmetry is significantly smaller than the region with six-fold symmetry.

It is useful to note that if the object is rotated, the outgoing OAM states simply pick up an overall phase that does not affect the joint OAM spectrum Fig. 5. This could be useful, because it allows a rapidly rotating object to be identified from its OAM spectrum using slow detectors and a small number of measurements. In some circumstances, this may be less expensive and more practical than the use of high speed cameras.
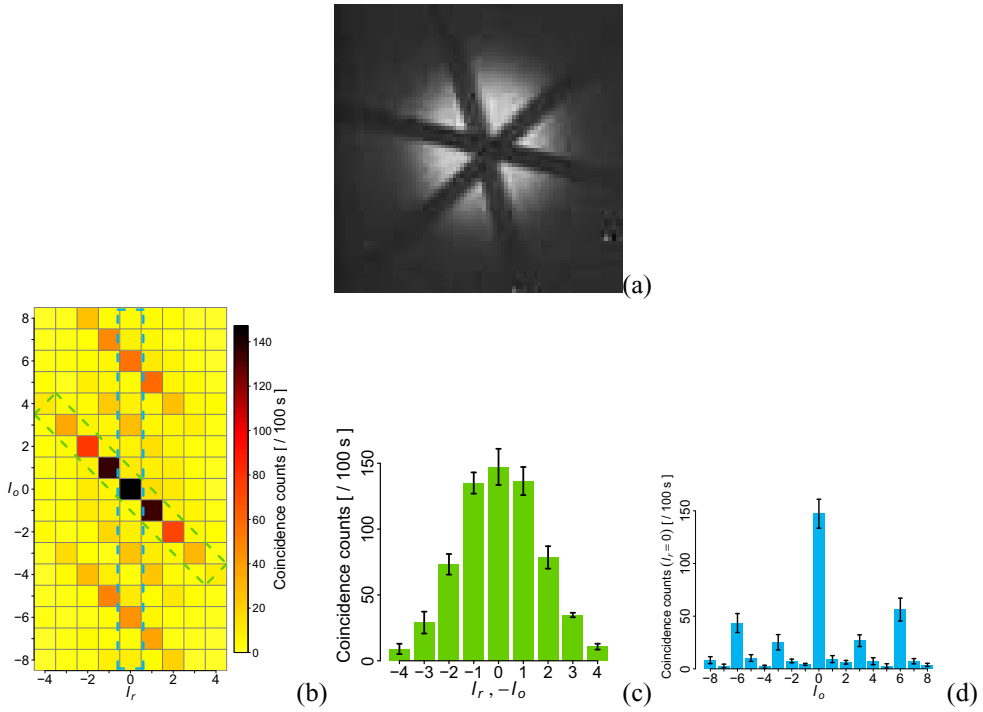
Figure 4. (a) Image of the three-arm cross used as target, (b) the experimental joint spectrum, (c) a histogram of the joint spectrum main diagonal and (d) $P(l_o|l_r = 0)$ cross section of the joint spectrum.

These results demonstrate that an object imprints its own characteristic features onto the OAM joint spectrum of SPDC as predicted by Eq. (8). New elements arise that do not fulfill the OAM conservation condition given by the OAM content of the pump alone but with the interaction with the object as well. The capability of CSI for object recognition is demonstrated by these results including high sensitivity to small symmetry components.

The high mutual information capacity of off-diagonal OAM spectral components also makes our method well suited for sensing rotational symmetries in few measurements. Due to the fragility of OAM states, the advantages of our setup may best be exploited in small scale biological or production
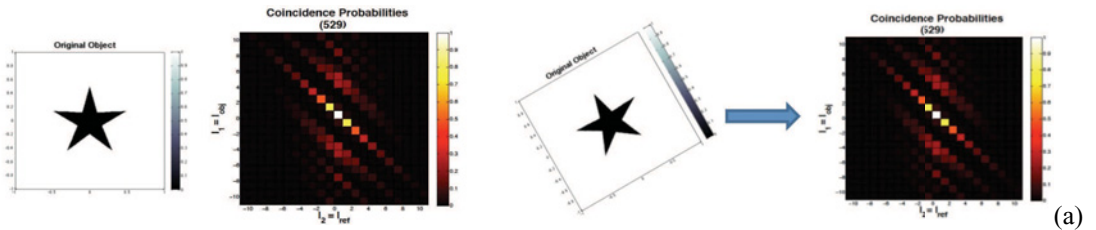

Figure 5. The rotation does not change the correlation matrix elements allowing for easy identification of rotating objects from the measured OAM spectrum.

contexts. For example, the scanning of a biological sample using correlated OAM measurements may enable efficient detection of the presence or absence of certain structures based on the comparison of theoretical and observed coincidence rates of off-diagonal spectral components.

Acknowledgements

References

[1] D.N. Klyshko, Sov. Phys. JETP **67**, 1131 (1988)
[2] A.V. Belinskii, D.N. Klyshko, Sov. Phys. JETP **78**, 259 (1994)
[3] T.B. Pittman, Y.H. Shih, D.V. Strekalov, A.V. Sergienko, Phys. Rev. A **52**, R3429 (1995)
[4] R.S. Bennink, S.J. Bentley, R.W. Boyd, Phys. Rev. Lett. **89**, 113601 (2002)
[5] E. Candes, M. Wakin, Signal Processing Magazine, IEEE **25**, 21 (2008)
[6] O. Katz, Y. Bromberg, Y. Silberberg, Applied Physics Letters **95**, 131110 (3) (2009)
[7] V. Katkovnik, J. Astola, J. Opt. Soc. Am. A **29**, 1556 (2012)
[8] B. Jack, J. Leach, J. Romero, S. Franke-Arnold, M. Ritsch-Marte, S.M. Barnett, M.J. Padgett, Phys. Rev. Lett. **103**, 083602 (2009)
[9] W. Gong, S. Han, J. Opt. Soc. Am. A **29**, 1571 (2012)
[10] L. Torner, J. Torres, S. Carrasco, Opt. Express **13**, 873 (2005)
[11] G. Molina-Terriza, L. Rebane, J.P. Torres, L. Torner, S. Carrasco, Journal of the European Optical Society: Rapid Publications **2** (2007)
[12] D.S. Simon, A.V. Sergienko, Phys. Rev. A **85**, 043825 (2012)
[13] J.P. Torres, A. Alexandrescu, L. Torner, Physical Review A **68**, 050301 (2003)
[14] X.F. Ren, G.P. Guo, B. Yu, J. Li, G.C. Guo, Journal of Optics B: Quantum and Semiclassical Optics **6**, 243 (2004)
[15] J. Leach, B. Jack, J. Romero, A.K. Jha, A.M. Yao, S. Franke-Arnold, D.G. Ireland, R.W. Boyd, S.M. Barnett, M.J. Padgett, Science **329**, 662 (2010)
[16] A. Mair, A. Vaziri, G. Weihs, A. Zeilinger, Nature **412**, 313 (2001)
[17] H. Di Lorenzo Pires, H.C.B. Florijn, M.P. van Exter, Physical Review Letters **104**, 020505 (2010)
[18] M. Padgett, L. Allen, Optics Communications **121**, 36 (1995)